Data-based modeling of drug penetration relates human skin barrier function to the interplay of diffusivity and free-energy profiles

Robert Schulz[a], Kenji Yamamoto[b], André Klossek[b], Roman Flesch[b], Stefan Hönzke[c], Fiorenza Rancan[d], Annika Vogt[d], Ulrike Blume-Peytavi[d], Sarah Hedtrich[c], Monika Schäfer-Korting[c], Eckart Rühl[b], and Roland R. Netz[a,1]

[a]Department of Physics, Freie Universität Berlin, 14195 Berlin, Germany; [b]Physical Chemistry, Freie Universität Berlin, 14195 Berlin, Germany; [c]Institute of Pharmacy, Freie Universität Berlin, 14195 Berlin, Germany; and [d]Clinical Research Center for Hair and Skin Science, Charité Clinic, 10117 Berlin, Germany

Based on experimental concentration depth profiles of the antiinflammatory drug dexamethasone in human skin, we model the time-dependent drug penetration by the 1D general diffusion equation that accounts for spatial variations in the diffusivity and free energy. For this, we numerically invert the diffusion equation and thereby obtain the diffusivity and the free-energy profiles of the drug as a function of skin depth without further model assumptions. As the only input, drug concentration profiles derived from X-ray microscopy at three consecutive times are used. For dexamethasone, skin barrier function is shown to rely on the combination of a substantially reduced drug diffusivity in the stratum corneum (the outermost epidermal layer), dominant at short times, and a pronounced free-energy barrier at the transition from the epidermis to the dermis underneath, which determines the drug distribution in the long-time limit. Our modeling approach, which is generally applicable to all kinds of barriers and diffusors, allows us to disentangle diffusivity from free-energetic effects. Thereby we can predict short-time drug penetration, where experimental measurements are not feasible, as well as long-time permeation, where ex vivo samples deteriorate, and thus span the entire timescales of biological barrier functioning.

diffusion | data-based modeling | biological barriers | skin | Smoluchowski equation

Multicellular organisms exhibit numerous structurally distinct protective barriers, such as the blood–brain barrier; intestinal, mouth, and respiratory mucosa; and the skin, the largest human organ. These barriers are generally designed to keep foreign material out and in some cases to allow the highly regulated transfer of certain desired molecules; consequently, they present a severe challenge for drug delivery (1–3). The in-depth understanding of barrier function is not only required for controlled drug delivery, but also of central interest in medicine, drug development, and biology.

Human skin can be broadly divided into two layers (Fig. 1*A*): the epidermis with a thickness of about 100 μm, which prevents water loss and the entrance of harmful microorganisms or irritants, and the dermis, which is typically 2 mm thick, contains blood vessels, and protects the body from mechanical stress (4). The epidermis is further divided into the stratum corneum (SC), the 10- to 20-μm thick outermost layer consisting of dried-out dead skin cells, the corneocytes, and the viable epidermis (VE). In the stratum granulosum (SG), which is part of the VE, skin cells (keratinocytes) are gradually flattened and transformed into corneocytes when migrating toward the SC.

The SC is structurally similar to a brick wall (5): The bricks are the corneocytes, whereas the mortar is the intercellular matrix, which is composed of stacked lipid bilayers. Several models for the permeation of drugs through skin exist,

which incorporate the skin structure on different levels of complexity. In the simplest models the stratified skin structure is reflected by 1D layers with different diffusivities and partition coefficients (6–10), and in more detailed models the 3D SC structure is accounted for (11, 12). In all models a certain skin structure and various transport parameters are assumed, which a posteriori are adjusted, such as to reproduce experimental permeabilities or concentration-depth profiles inferred from tape-stripping studies (11, 12). For a detailed overview of skin-diffusion models and a historical outline see refs. 13 and 14.

We describe here a data-based modeling approach, i.e., which does not make any model assumptions and as the only input requires drug concentration-depth profiles in the skin at three consecutive times. Our approach, which we test for the lipophilic antiinflammatory glucocorticoid dexamethasone (DXM) in ex vivo human skin, is very general and can be used for all kinds of permeation barriers. This drug is chosen because soft X-ray absorption spectromicroscopy allows us to generate 2D absolute concentration profiles of unlabeled DXM in thin skin slabs with a resolution below 100 nm (15, 16).

We start with the general 1D diffusion equation, which describes the evolution of a 1D concentration profile $c(z, t)$ in space and time and depends on the position-dependent free-energy profile $F(z)$ and the diffusivity profile $D(z)$,

---

Significance

Human skin consists of distinct layers and is designed to prevent water loss and to keep harmful materials out, which makes transcutaneous drug delivery challenging. A model for drug diffusion within skin is introduced that as the only input requires experimental concentration profiles measured at three distinct penetration times. For the specific example of the antiinflammatory drug dexamethasone, the modeling shows that both free-energy and diffusivity profiles are highly inhomogeneous, which reveals the basic mechanism of epidermal barrier function: slow diffusion in the outer stratum corneum hinders fast penetration into the skin, whereas a pronounced free-energy step from the epidermis to the dermis underneath reduces long-time permeation. Targeted drug delivery strategies through skin must reflect these properties.

BIOPHYSICS AND COMPUTATIONAL BIOLOGY

APPLIED PHYSICAL SCIENCES

$$\frac{\partial}{\partial t} c(z,t) = \frac{\partial}{\partial z}\left(D(z) e^{-\beta F(z)} \frac{\partial}{\partial z} c(z,t) e^{\beta F(z)} \right), \quad [1]$$

where $\beta = 1/(k_B T)$ is the inverse thermal energy. The free-energy profile $F(z)$ reflects the local affinity and determines how the substance, in our specific case DXM, partitions in equilibrium, namely $c_{eq}(z) \propto e^{-\beta F(z)}$. The diffusivity profile $D(z)$ is a local measure of the velocity at which the substance diffuses in the absence of external forces. The diffusion equation not only describes passive and active particle transport in structured media, it has in the past also been used for modeling marketing strategies (17), decision making (18), and epigenetic phenotype fluctuations (19). The importance of a spatially varying diffusivity profile $D(z)$ has been recognized for the relative diffusion of two particles (20), transmembrane transport (21), particle diffusion at interfaces (22, 23), protein folding (24–27), and multidimensional diffusion (28). The 1D diffusion equation can be solved analytically only in simple limits; for general $F(z)$ and $D(z)$ profiles the solution $c(z,t)$ must be numerically calculated.

The inverse problem, i.e., extracting $F(z)$ and $D(z)$ from simulation or experimental data, is much more demanding and has recently attracted ample theoretical attention. With one notable exception (29), most inverse approaches need single-particle stochastic trajectories and are not suitable to extract information from concentration profiles (20–22, 30–32). For the typical experimental scenario, where a few concentration profiles at different times are available, we here present a robust method that yields the $F(z)$ and $D(z)$ profiles with minimal numerical effort and for general open boundary conditions (*Materials and Methods*). We demonstrate our method using experimental 1D concentration-depth profiles of DXM, a medium-size drug molecule that in water is only poorly soluble (33). Starting the drug penetration by placing a 1.5% DXM formulation in a hydroxyethyl cellulose (HEC) gel on top of excised human skin at time 0, 2D concentration profiles of DXM in the epidermal skin layer are obtained after penetration times of 10 min, 100 min, and 1,000 min, using soft X-ray absorption spectromicroscopy (15, 16) (*Materials and Methods*).

To determine both the free-energy profile $F(z)$ and the diffusivity profile $D(z)$ in the epidermal skin layer as well as the diffusive DXM properties in the drug-containing HEC gel and in the dermis, we need three experimental concentration profiles recorded at different times as input. We demonstrate that both the diffusivity profile $D(z)$, which dominates drug penetration for short times, and the free-energy profile $F(z)$, which dominates long-time drug concentration profiles, are needed to describe drug penetration quantitatively.

Our analysis reveals that skin barrier function results from an intricate interplay of different skin layer properties: Whereas the entrance of lipophilic DXM into the SC is free-energetically favored, the drug diffusivity in the SC is about 1,000 times lower than in the VE and thus slows down the passage of DXM through the SC. In addition, a pronounced free-energy barrier from the epidermis to the dermis prevents DXM from penetrating into the lower dermal layers. In essence, the epidermis has a high affinity for the lipophilic drug DXM, which together with the low diffusivity in the SC efficiently prevents DXM penetration into the dermis.

Results and Discussion

Experimental Concentration Profiles. Fig. 1*B* shows 2D absorption profiles recorded at photon energy 530.1 eV for penetration times of 10 min, 100 min, and 1,000 min. This photon energy selectively excites DXM (15). The skin-depth coordinate z is shifted such that the outer skin surface is aligned to $z = 0$. The color codes the transmitted intensity, with blue indicating low and yellow high transmission, and allows insights into the skin structure. Note that the three profiles originate from different skin samples from the same donor, because the analysis of the identical skin sample for different penetration times is not possible (16). Accordingly, these three samples have been chosen for maximal similarity of the SC and VE thicknesses.

The region below $z < 0$ μm is the Epon resin used for skin embedding. For all three samples, the layered structure from $z \approx 0$ μm to $z \approx 10$ μm is the SC, whereas the VE extends from a depth of about $z \approx 10$ μm to a variable depth ranging from $z \approx 50$ μm to $z \approx 80$ μm. Within the VE oval-shaped keratinocyte nuclei are discerned, which move gradually toward the SC where they differentiate and flatten into corneocytes. The dermis, separated from the VE by the basal layer and the basal membrane, is clearly distinguished from the VE by the different transmission intensity. Note that the variation of the VE thickness across different samples is an inherent property of skin and must be kept in mind in the analysis. From the ratio of the 2D transmission profiles at photon energies of 530.1 eV and 528.0 eV the 2D concentration profiles of DXM are determined (15, 16) (see *Materials and Methods*, *DXM Concentration Profiles from X-Ray Microscopy*, and Figs. S1 and S2 for details).

Our aim is not to describe DXM diffusion at the cellular level, for which 3D concentration profiles at different penetration times of the same sample would be needed; our goal rather is to model the 1D diffusion of DXM from the HEC gel on the skin surface through the epidermis into the deeper skin layers. For this, we laterally average the experimental 2D concentration profiles; the resulting 1D concentration data are shown in Fig. 2*A* (black solid circles). We base our modeling on cubic smoothing spline fits (black lines) in the range $0 < z < 80$ μm,
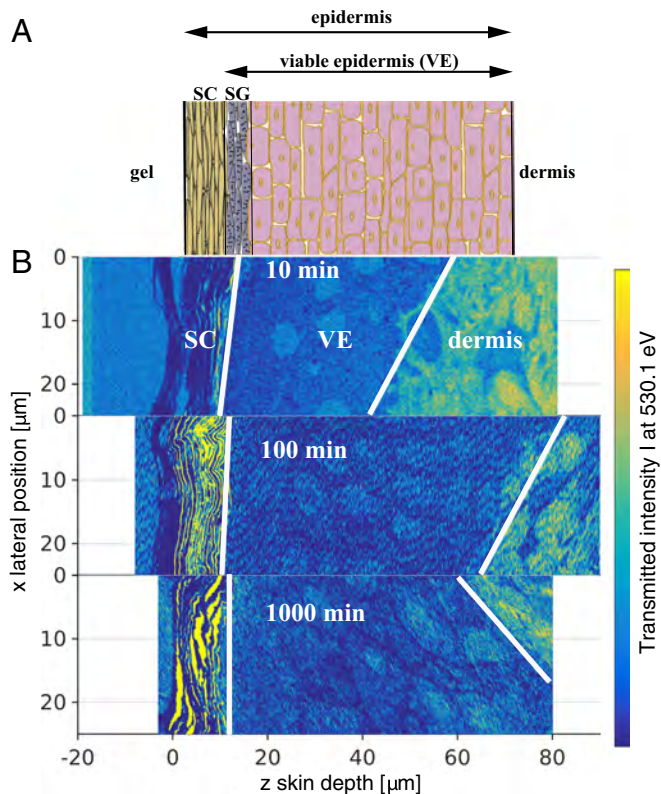

Fig. 1. (*A*) Schematic of epidermal skin structure. (*B*) Normalized 2D-transmission intensity profiles from X-ray scanning microscopy at photon energy 530.1 eV after 10 min, 100 min, and 1,000 min penetration time. The profiles allow us to distinguish different skin layers, schematically indicated by white dividing lines, and demonstrate the skin sample variation. Whereas the SC has a rather uniform thickness, the VE thickness varies considerably between the three samples.
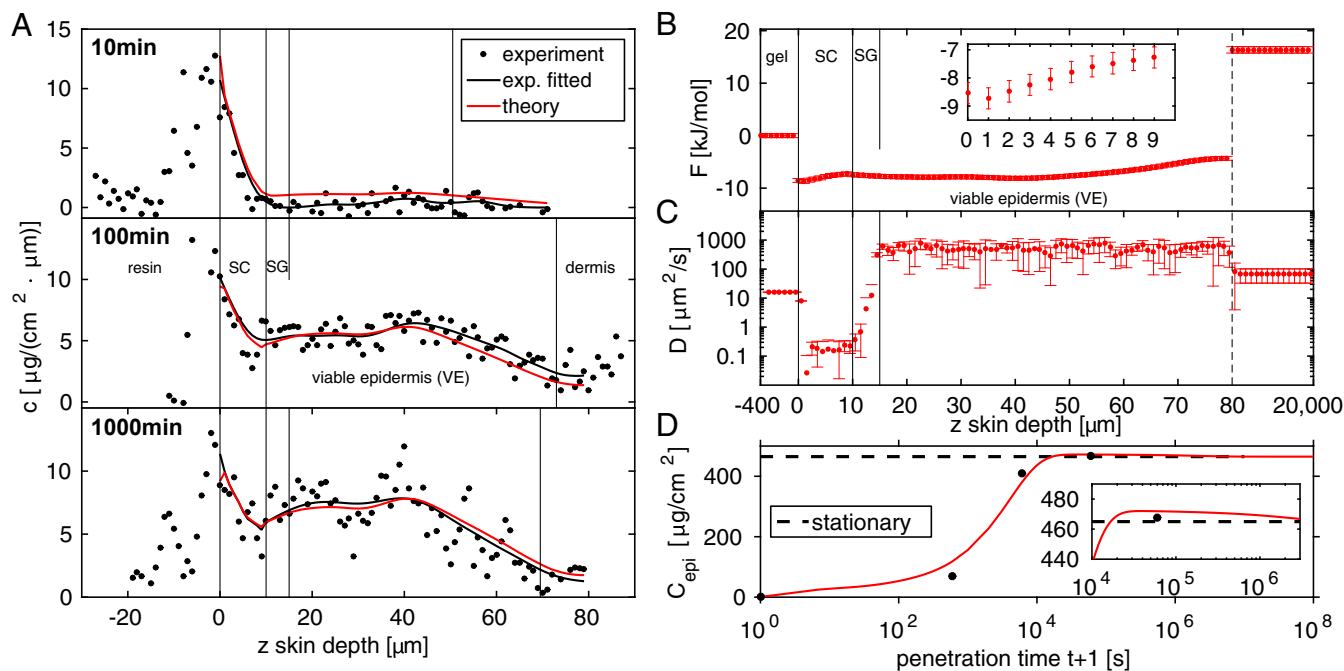
Fig. 2. (A) One-dimensional experimental DXM concentration profiles at three different penetration times (black solid circles) and cubic smoothing splines (black lines) are compared with theoretical predictions based on the diffusion equation (red lines). Vertical dividing lines indicate skin layers and are based on the 2D transmission intensity profiles in Fig. 1B. (B and C) Free-energy profile $F(z)$ (B) and diffusivity profile $D(z)$ (C) derived from the experimental concentration profiles. $F(z)$ is low in the entire epidermis (SC and VE) compared to the HEC gel and to the dermis and exhibits a small but significant gradual increase in the SC (B, *Inset*), and the epidermis thus exhibits lipophilic affinity. $D(z)$ is low in the SC and increases by a factor of 1,000 in the VE, where it is close to the free-solution value. The low diffusivity in the SG in the depth range 10 μm $< z <$ 15 μm could indicate the presence of tight junctions. In the gel and beyond $z = 80$ μm (indicated by a vertical dashed line) the $F(z)$ and $D(z)$ profiles are approximated as constant. (D) Integrated amount of DXM in the epidermis C_{epi} from experiments (black solid circles) and theory (red line), showing a maximum at penetration time $t \approx 6 \times 10^4$ s = 1,000 min (*Inset*) before it relaxes to the predicted stationary value indicated by a horizontal dashed line.

disregarding residual DXM in the Epon resin for $z < 0$ μm as well as the range $z > 80$ μm where only a single concentration profile is available. It is seen that already after 10 min penetration DXM has entered the SC. After 100 min penetration DXM is found in the VE, whereas the concentration in the SC has not changed much. The difference between the 100-min and the 1,000-min profiles is seen to be rather small.

Extracting Free-Energy and Diffusivity Profiles. Feeding the three experimental DXM concentration profiles in the depth range $0 < z < 80$ μm after 10 min, 100 min, and 1,000 min penetration time into our inverse solver for the diffusion equation, we derive the best estimates for the $F(z)$ and $D(z)$ profiles shown in Fig. 2 *B* and *C*; in the gel and in the dermis, due to the absence of experimental data, we approximate $F(z)$ and $D(z)$ to be constant. The error bars reflect the SD of the estimates that pass the error threshold $\sigma < 0.6$ μg/(cm²·μm) (see *Materials and Methods* for more details).

The free energy $F(z)$ in Fig. 2B, approximated to be constant in the gel and set to $F_{gel} = 0$, exhibits a jump down by $\Delta F_{gel/SC} \approx -8.6$ kJ/mol at the boundary between gel and SC. This is in line with the lipophilic character of DXM, which prefers to be in the lipid-rich SC compared with the HEC gel formulation. In the SC, the free energy increases rather smoothly by ≈ 1.5 kJ/mol over a range of 10 μm (Fig. 2B, *Inset*), reflecting a significant structural change across the SC that sustains the steep water chemical potential gradient across the SC (34). In the depth range 10 μm $< z <$ 50 μm, which corresponds to the VE, the free energy is rather constant. In the range 50 μm $< z <$ 80 μm the free energy slightly increases again, which reflects the decreasing DXM concentration in the experimental profiles in Fig. 2A for 100 min and 1,000 min. Compar-

ison with the transmission intensity profiles in Fig. 1B reveals that this free-energy increase is caused by the transition from the epidermis to the dermis, which due to skin sample variations is smeared out over a broad depth range of 50 μm $< z <$ 80 μm. The free-energy jump of $\Delta F_{VE/derm} \approx 20.5$ kJ/mol at $z = 80$ μm reflects a pronounced barrier for DXM penetration into the dermis related to the different DXM affinity to the dermis compared with the VE. Due to data scattering this value constitutes a lower bound, as is explained in *Estimate of Free-Energy Barrier Height Between Epidermis and Dermis* and Fig. S3. In fact, the free-energy difference between the HEC gel and the dermis, $\Delta F_{gel/derm} \approx 16.2$ kJ/mol = 6.4 $k_B T$, is quite close to the free-energy difference derived from the maximal DXM solubility in water, $c_{H_2O} = 89$ mg/L at 25 °C (35), and the DXM solubility in the HEC gel $c_{gel} = 15$ g/L, via the partition coefficient according to $k_B T \ln(c_{gel}/c_{H_2O}) = 5.1 k_B T$. The free-energy profile thus identifies the dermis as essentially water-like, whereas the epidermis is a sink with high lipophilic affinity, in line with previous conclusions (36).

The constant diffusivity in the HEC gel turns out to be $D_{gel} \approx 16$ μm²/s and drops in the SC by a factor of roughly 80 to $D_{SC} \approx 0.2$ μm²/s (Fig. 2C). The diffusivity maintains such a low value up to a depth of $z = 15$ μm, where it abruptly increases. For $z \geq 15$ μm $D(z)$ exhibits a rather constant value of $D_{VE} \approx 400$ μm²/s, which is significantly larger than the value in the HEC gel and somewhat smaller than the estimated diffusion constant of dexamethasone in pure water, $D_{H_2O} \approx 680$ μm²/s (33). We tentatively associate the layer 10 μm $< z <$ 15 μm, where the diffusivity is as low as in the SC but structurally is distinct from the SC and belongs to the VE, with the SG. Note that the SG, which is known to be located right below the SC, is not visible in the transmission profiles in Fig. 1. The SG barrier

function has been shown to be due to tight junctions (37–40), in line with the low local diffusivity in this region displayed in Fig. 2*C*.

Summarizing, four distinct features are revealed by our analysis: (*i*) a low diffusivity in the SC, (*ii*) a low diffusivity in a thin layer just below the SC that we associate with the SG, (*iii*) a sudden drop in free energy from the gel to the SC and a slight but significant free-energy increase in the SC, and (*iv*) a pronounced free energy barrier from the epidermis to the dermis. We stress that these features in the free-energy and diffusivity profiles are not put in by way of our analysis method, but rather directly follow from the experimental concentration profiles. We note in passing that the steep increase of the diffusivity at the boundary from the putative SG (with $D_{SG} \approx 1$ μm²/s) to the VE (with $D_{VE} \approx 400$ μm²/s) is nothing one could directly identify from the experimental concentration profiles shown in Fig. 2*A*.

Predicting Concentration Profiles. In Fig. 2*A* we demonstrate that the numerical solutions of the diffusion equation (red lines), based on the free-energy and diffusivity profiles $F(z)$ and $D(z)$ in Fig. 2 *B* and *C*, reproduce the experimental concentration profiles very well (black lines). Small deviations are observed for the drug-concentration profile after 10 min penetration time, and the agreement is almost perfect for the 100-min and 1,000-min profiles. This not only means that our method for extracting $F(z)$ and $D(z)$ from concentration profiles works; we also conclude that the diffusion equation Eq. **1** describes the concentration time evolution in skin very well.

We define the time-dependent integral DXM amount that has penetrated into the epidermis over the distance range $0 < z < 80$ μm as

$$C_{epi} = \int_{0 \text{ μm}}^{80 \text{ μm}} c(z)\,dz. \qquad [2]$$

In Fig. 2*D* we compare the experimental data for C_{epi} (solid black circles), which are directly obtained by integrating over the experimental concentration profiles in Fig. 2*A*, with the theoretical prediction based on the diffusion equation and the determined $F(z)$ and $D(z)$ profiles (red line). Note the logarithmic timescale that extends from $t = 1$ s to $t = 10^8$ s ≈ 3 y. According to the experimental protocol, at time $t = 0$ the entire amount of DXM, corresponding to a surface concentration of 600 μg/cm², is located in the gel and thus C_{epi} is zero. With increasing time, the theoretically predicted C_{epi} increases gradually and reaches a maximum of $C_{epi} = 471.9$ μg/cm² at $t \approx 6 \times 10^4$ s = 1,000 min, at which time only ≈ 1.2 μg/cm² DXM has penetrated into the dermis [*Calculating the DXM Penetration Amount from Estimated F(z) and D(z) Profiles*]. In the long-time limit, which is reached above $t \approx 10^7$ s ≈ 115 d, as seen in Fig. 2*D*, *Inset*, theory predicts the equilibrium value $C_{epi}^{eq} = 465.0$ μg/cm², denoted by a horizontal dashed line. In this hypothetical limit, longer than the exfoliation time of skin, which is 30–40 d, theory predicts that ≈ 10.0 μg/cm² DXM has penetrated into the dermis, whereas ≈ 125.0 μg/cm² DXM still resides in the gel [see *Calculating the DXM Penetration Amount from Estimated F(z) and D(z) Profiles* for the full calculation]. Note that in vivo, dermal blood perfusion is crucial and could be easily taken into account in a generalized diffusion model by an additional reaction term.

The theoretically predicted curve for C_{epi} in Fig. 2*D* agrees well with the experimental data, which is not surprising in light of the good agreement of the concentration profiles in Fig. 2*A*. This indicates that also the short- and long-time DXM penetration amounts, which are difficult to extract experimentally, are straightforwardly obtained from our model.

In Fig. 3 we show calculated DXM concentration depth profiles for a wide range of times. We here also plot the predicted concentration profiles in the gel and below the epidermis, for
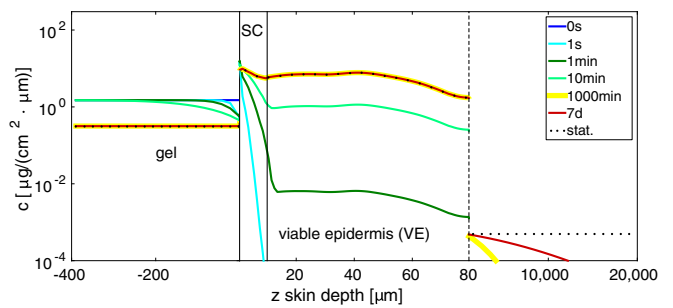

Fig. 3. Comparison of theoretical DXM concentration profiles for a wide range of different penetration times. At time 0 the drug is entirely in the gel. Already at $t = 1$ s DXM penetrates into the SC. At intermediate times $t = 1$ min and $t = 10$ min the VE is gradually filled, whereas at longer times $t = 1,000$ min and $t = 7$ d the profile below the epidermis approaches the stationary profile (indicated by a dotted curve).

which no experimental data are available. We see that for short penetration times the concentration profile in the HEC gel is inhomogeneous, so the simplifying assumption of a constant concentration in the gel becomes invalid. Interestingly, already at $t = 1$ s DXM enters the SC. The 1,000-min profile is indistinguishable from the stationary profile in the HEC gel and the epidermis, whereas below the epidermis, extending from $z = 80$ μm to $z = 2$ cm, even after 7 d the stationary (flat) concentration profile has not yet been reached (note the inhomogeneous depth scale and the logarithmic concentration scale). Not surprisingly, molecular diffusion over a macroscopic length scale of 2 cm takes a long time.

Checking Model Validity. We check the robustness of our diffusion model by comparison with two simplified models. In the constant-F model we restrict the free energy in the epidermis to be constant (with the diffusivity still being a variable function), whereas in the constant-D model we restrict the diffusivity in the epidermis to be constant (with the free energy being a variable function). This means that the number of adjustable model parameters drops from 162 in the full model down to 83; otherwise we use the same methods for finding inverse solutions of the diffusion equation as before (*Materials and Methods*).

The free-energy profiles of the constant-F (blue) and the constant-D (green) models in Fig. 4*A* are rather similar and do not differ much from the full model result (red); in particular, the free-energy jumps from the HEC gel to the SC and from the VE to the dermis come out roughly the same. The diffusivity profile of the constant-F model in Fig. 4*B* is again similar to the full model, whereas the constant-D model obviously misses the diffusivity jump from the SC to the VE region.

When we look at the predicted DXM concentration profiles in Fig. 4*C*, we clearly see the shortcomings of the restricted models: The constant-F model (blue lines) correctly predicts the short-time behavior including the 10-min profile, but fails severely for the long penetration time of 1,000 min, which is close to the stationary equilibrium limit. In contrast, the constant-D model (green line) produces a concentration profile for 1,000 min that is indistinguishable from the full model and thus describes the experimental profile very nicely, whereas it fails at the short penetration time of 10 min. The comparison of the full model to the restricted models demonstrates that both the free-energy and the diffusivity profiles are needed to correctly describe the experimental concentration profiles over the entire penetration time range from 10 min to 1,000 min. We also understand from this comparison that the diffusivity profile is important at penetration times up to 10 min, whereas the free-energy profile is required to describe the long-time and the equilibrium behavior accurately.
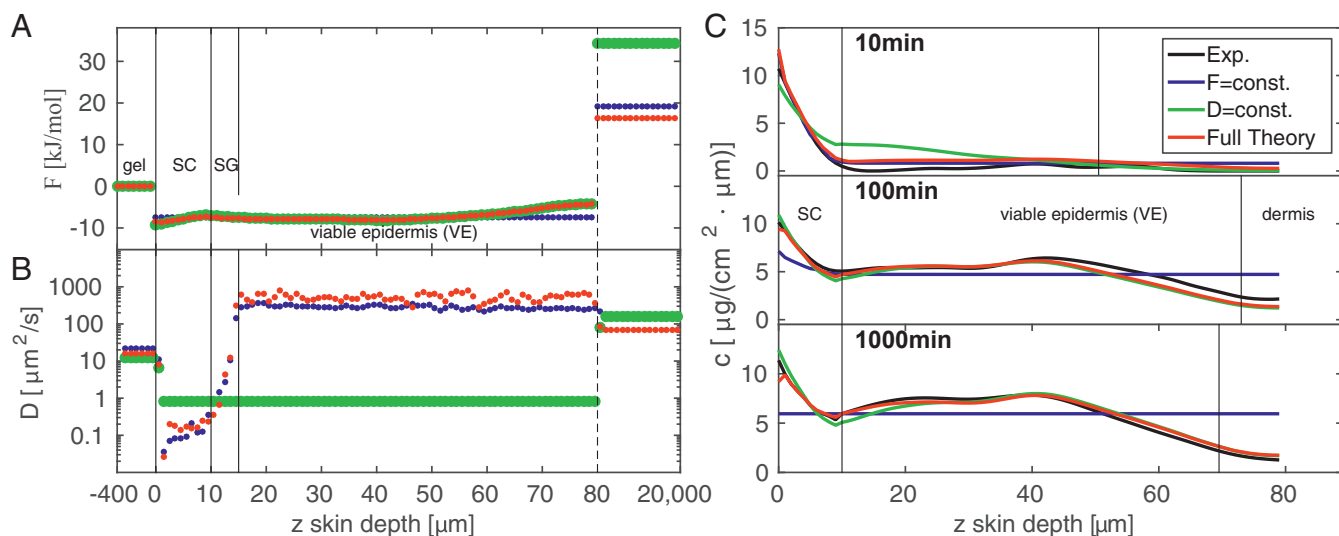
Fig. 4. (*A*–*C*) Comparison of the restricted constant-F (blue lines) and the constant-D (green lines) models to the full model (red lines) and experimental concentration profiles (black lines) in terms of the (*A*) free-energy, (*B*) diffusivity, and (*C*) concentration profiles. The constant-F model fails to predict the experimental long-time concentration profiles for penetration times 100 min and 1,000 min, and the constant-D model fails to predict the short-time concentration profile 10 min.

A robustness check by comparison with results obtained from a reduced dataset is shown in *Bootstrapping Analysis* and *Fig. S4*, from which we conclude that the model is able to correctly predict concentration profiles even for times at which limited data are provided.

Conclusions

A method for deriving free-energy and diffusivity profiles from experimental concentration profiles at three different penetration times of drugs in human skin is presented. The approach is generally applicable to all kinds of barrier situations and different diffusors whenever spatially resolved concentration profiles at different times are available and can also be generalized to higher dimensions. For the specific example of DXM penetrating into human skin, our results demonstrate that both diffusivity and free-energy profiles are important to describe the skin barrier: The inhomogeneous free-energy profile is essential to correctly describe the long-time concentration profiles, whereas the diffusivity profile is needed for reproducing the short-time drug penetration. Epidermal skin barrier function against the permeation of DXM is shown to rely on the combination of two key properties, namely a low diffusivity in the SC and a low free energy (i.e., high solubility) in the entire epidermis. Each of these properties by itself severely reduces the DXM permeation through the epidermis, but it is the combination that leads to the exceptionally low and slow DXM transport into the dermis.

The design of efficient drug delivery methods through the epidermis thus meets two challenges: First, the low diffusivity in the SC needs to be overcome. And second, the free-energy barrier from the epidermis, which we show to have pronounced lipophilic affinity, to the hydrophilic dermis severely slows down the permeation of lipophilic drugs. The remedy could consist of modified drugs with balanced lipophilic–hydrophilic character such that the epidermis–dermis affinity barrier is small or even absent.

Materials and Methods

Experimental Concentration Profiles. Our studies were detailed previously (15, 16) and use ex vivo human 2-cm-thick abdominal skin samples. The study was approved by the Ethics Committee of the Charité Clinic Berlin (approval EA/1/135/06, updated July 2015). It was in accordance with the Declaration of Helsinki guidelines and the samples were obtained after the signed con-

sent of the patients. The skin surface was exposed to a 0.4-mm-thick layer of a 70% ethanol HEC gel formulation containing DXM with a concentration of $c_{gel}(t = 0) = 1.5$ mg/(cm²·mm) for penetration times of 10 min, 100 min, and 1,000 min at a temperature of 305 K in a humidified chamber at the saturation point. After gently removing the HEC gel, samples were subsequently treated in 2.5% glutaraldehyde in 0.1 M Na-cacodylate buffer and with K$_4$[(Fe(CN)$_6$] and OsO$_4$ for lipid and DXM fixation, dehydrated, embedded in epoxy resin, sliced into sections of 350-nm thickness, and placed on silicon nitride membranes of 100-nm thickness. X-ray microscopy studies were performed at the synchrotron radiation facility BESSY II (Berlin, Germany) in a scan depth range of 100 μm with a step width of 200 nm. The photon energy was tuned to probe exclusively DXM at 530.1 eV via the O $1s \rightarrow \pi^*$ transition (16). This allows us to derive the absolute local DXM concentration by using Beer–Lambert's law; see refs. 15 and 16 for details.

Numerical Solution and Inversion of Diffusion Equation. For the numerical solution the diffusion Eq. 1 is discretized in space and time and takes the form of a Master equation (41)

$$\frac{c_i(t + \Delta t) - c_i(t)}{\Delta t} = W_{i,i-1}c_{i-1}(t) + W_{i,i+1}c_{i+1}(t) + W_{i,i}c_i(t), \quad [3]$$

where Δt is the time discretization step. We match different spatial discretization schemes: Because experimental concentration data are available at micrometer resolution in the epidermis up to a skin depth of 80 μm, we use an equidistant discretization with $\Delta z = 1$ μm in the range $0 < z < 80$ μm. For the transition rates we use (41)

$$W_{i,j} = \frac{D_i + D_j}{2(\Delta z)^2} \exp\left(-\frac{F_i - F_j}{2 k_B T}\right) \quad \text{with} \quad j = i \pm 1 \quad [4]$$

and $W_{i,i} = -W_{i-1,i} - W_{i+1,i}$, which satisfies concentration conservation and detailed balance. We thus have $2 \times 80 = 160$ parameters from the discretized $F(z)$ and $D(z)$ profiles in the epidermal layer. In the HEC gel, which serves as the DXM source during the penetration, no experimental concentration data are available. We discretize the HEC gel with seven sites and a total thickness of 0.4 mm, as in the experiment. We discretize the dermis and the subcutaneous layer, for which also no experimental concentration data are available, with 15 sites and a total thickness of 2 cm, as in the experiment. The total number of discretization sites is $N = 102$. The free energies F_{gel} and F_{derm} and the diffusivities D_{gel} and D_{derm} in the HEC gel and the subepidermal layer are assumed to be constant and are treated as free-fitting parameters. Reflective boundary conditions are used at the upper gel surface and at the lower subdermal boundary, as appropriate for the experimental conditions. The total number of parameters is reduced from 164 to 162 due to the fact that only free-energy differences and diffusivity sums of neighboring sites enter Eq. 4. For more details see *Variable Discretization of the 1D*

BIOPHYSICS AND COMPUTATIONAL BIOLOGY

APPLIED PHYSICAL SCIENCES

Diffusion Equation. The concentration profile $c_i(t)$ at time $t = n\Delta t$ follows from Eq. **3** as

$$c_i(t) = \sum_{j=1}^{N} \left[(\mathbb{1} + \Delta t \mathbb{W})^n \right]_{i,j} c_j(0) = \sum_{j=1}^{N} e_{i,j}^{t\mathbb{W}} c_j(0), \qquad [5]$$

where $\mathbb{W}$ is the rate matrix defined in Eq. **4** and the continuous limit $\Delta t \to 0$ has been taken to express the nth power by the matrix exponential. Eq. **5** can be used to numerically solve the diffusion equation for any initial distribution $c_j(t=0)$ and diffusivity and free-energy profiles $D(z)$ and $F(z)$. To determine $D(z)$ and $F(z)$ based on experimental concentration profiles at different times, we minimize the squared sum of deviations

$$\sigma^2 = \frac{1}{N_p} \sum_{k=1}^{N_p} \frac{1}{N_k^{\text{data}}} \sum_{i=1}^{N_k^{\text{data}}} \left(c_i^{\exp}(t_k) - \sum_{j=1}^{N} e_{i,j}^{t_k \mathbb{W}} c_j(0) \right)^2, \qquad [6]$$

where N_k^{data} is the number of experimental concentration data per profile and $N_p = 3$ is the number of experimental concentration profiles. We use $N_1^{\text{data}} = 73$ data points for the 10-min profile and $N_2^{\text{data}} = N_3^{\text{data}} = 80$ data points for the 100-min and 1,000-min profiles, taken from the smoothed splines (black lines) in Fig. 2*A*. The total number of $233 = 73 + 80 + 80$ input data points is necessarily higher than the number of 162 free-energy and diffusivity parameters we need to determine. The profile $c_i(t=0)$ corresponds to the initial condition where DXM is homogeneously distributed in the gel only. For minimization of the error function Eq. **6** we use the trust-region iteration approach (42, 43); see *Trust-Region Optimization for Constrained Nonlinear Problems* for details. As an initial guess for the minimization we use a flat free-energy profile and choose random values for $D(z)$ in the range $[10^{-1}, \ldots, 10^3]\ \mu m^2/s$. We perform 1,000 runs with different initial values for $D(z)$ with a maximal number of 250 iterations per run. For our results, we use only the best 1% of solutions with a residual error $\sigma < 0.6\ \mu g/(cm^2 \cdot \mu m)$. A perfect solution with an error of $\sigma = 0$ is never observed, which reflects that our equation system is overdetermined and at the same time input concentration profiles come from different skin samples. In the constant-F and constant-D models we obtains errors $\sigma < 1.6\ \mu g/(cm^2 \cdot \mu m)$ and $\sigma < 0.9\ \mu g/(cm^2 \cdot \mu m)$ for the best 1% of the solutions, significantly larger than for the full model.

1. Cevc G, Vierl U (2010) Nanotechnology and the transdermal route: A state of the art review and critical appraisal. *J Control Release* 141(3):277–299.
2. Lieleg O, Ribbeck K (2011) Biological hydrogels as selective diffusion barriers. *Trends Cell Biol* 21(9):543–551.
3. Blanco E, Shen H, Ferrari M (2015) Principles of nanoparticle design for overcoming biological barriers to drug delivery. *Nat Biotechnol* 33(9):941–951.
4. Schaefer H, Zesch A, Stüttgen G (1982) *Skin Permeability* (Springer, Berlin).
5. Elias P (1991) Epidermal barrier function - intercellular lamellar lipid structures, origin, composition and metabolism. *J Control Release* 15(3):199–208.
6. Bhatt PP, Hanna MS, Szeptycki P, Takeru H (1989) Finite dose transport of drugs in liquid formulations through stratum corneum: Analytical solution to a diffusion model. *Int J Pharm* 50(3):197–203.
7. Kubota K (1991) Finite dose percutaneous drug absorption: A basic program for the solution of the diffusion equation. *Comput Biomed Res* 24(2):196–207.
8. Anissimov YG, Roberts MS (2000) Diffusion modeling of percutaneous absorption kinetics. 1. Effects of flow rate, receptor sampling rate, and viable epidermal resistance for a constant donor concentration. *J Pharm Sci* 89(1):144–144.
9. Kasting GB (2001) Kinetics of finite dose absorption through skin 1. Vanillylnonanamide. *J Pharm Sci* 90(2):202–212.
10. Kasting GB, Miller MA (2006) Kinetics of finite dose absorption through skin 2: Volatile compounds. *J Pharm Sci* 95(2):268–280.
11. Rim JE, Pinsky PM, van Osdol WW (2008) Using the method of homogenization to calculate the effective diffusivity of the stratum corneum with permeable corneocytes. *J Biomech* 41(4):788–796.
12. Naegel A, et al. (2011) Finite dose skin penetration: A comparison of concentration-depth profiles from experiment and simulation. *Comput Vis Sci* 14(7):327–339.
13. Naegel A, Heisig M, Wittum G (2013) Detailed modeling of skin penetration - an overview. *Adv Drug Deliv Rev* 65(2):191–207.
14. Mitragotri S, et al. (2011) Mathematical models of skin permeability: An overview. *Int J Pharm* 418(1):115–129.
15. Yamamoto K, et al. (2015) Selective probing of the penetration of dexamethasone into human skin by soft x-ray spectromicroscopy. *Anal Chem* 87(12):6173–6179.
16. Yamamoto K, et al. (2016) Core-multishell nanocarriers: Transport and release of dexamethasone probed by soft x-ray spectromicroscopy. *J Control Release* 242:64–70.
17. Bass FM (1969) A new product growth for model consumer durables. *Manag Sci* 15(5):215–227.
18. Ratcliff R, McKoon G (2008) The diffusion decision model: Theory and data for two-choice decision tasks. *Neural Comput* 20(4):873–922.
19. Sisan D, Halter M, Hubbard J, Plant A (2012) Predicting rates of cell state change caused by stochastic fluctuations using a data-driven landscape model. *Proc Natl Acad Sci USA* 109(47):19262–19267.
20. Straub J, Berne B, Roux B (1990) Spatial dependence of time-dependent friction for pair diffusion in a simple fluid. *J Chem Phys* 93(9):6804–6812.
21. Marrink SJ, Berendsen H (1994) Simulation of water transport through a lipid membrane. *J Phys Chem* 98(15):4155–4168.
22. Liu P, Harder E, Berne B (2004) On the calculation of diffusion coefficients in confined fluids and interfaces with an application to the liquid-vapor interface of water. *J Phys Chem B* 108(21):6595–6602.
23. Bollinger J, Jain A, Truskett T (2014) Structure, thermodynamics, and position-dependent diffusivity in fluids with sinusoidal density variations. *Langmuir* 30(28):8247–8252.
24. Bryngelson J, Wolynes P (1989) Intermediates and barrier crossing in a random energy model (with applications to protein folding). *J Phys Chem* 93(19):6902–6915.
25. Krivov S, Karplus M (2008) Diffusive reaction dynamics on invariant free energy profiles. *Proc Natl Acad Sci USA* 105(37):13841–13846.
26. Best R, Hummer G (2010) Coordinate-dependent diffusion in protein folding. *Proc Natl Acad Sci USA* 107(3):1088–1093.
27. Chung H, Piana-Agostinetti S, Shaw D, Eaton W (2015) Structural origin of slow diffusion in protein folding. *Science* 349(6255):1504–1510.
28. Berezhkovskii A, Szabo A (2011) Time scale separation leads to position-dependent diffusion along a slow coordinate. *J Chem Phys* 135(7):074108–074112.
29. Lund SP, Hubbard JB, Halter M (2014) Nonparametric estimates of drift and diffusion profiles via Fokker-Planck algebra. *J Phys Chem B* 118(44):12743–12749.
30. Hummer G (2005) Position-dependent diffusion coefficients and free energies from Bayesian analysis of equilibrium and replica molecular dynamics simulations. *New J Phys* 7:516–523.
31. Hinczewski M, von Hansen Y, Dzubiella J, Netz RR (2010) How the diffusivity profile reduces the arbitrariness of protein folding free energies. *J Chem Phys* 132(24):245103–245112.
32. Carmer J, van Swol F, Truskett T (2014) Note: Position-dependent and pair diffusivity profiles from steady-state solutions of color reaction-counterdiffusion problems. *J Chem Phys* 141(4):046101–046102.
33. Moussy Y, Hersh L, Dungel P (2006) Distribution of [3H]dexamethasone in rat subcutaneous tissue after delivery from osmotic pumps. *Biotechnol Prog* 22(3):819–824.
34. Sparr E, Wennerström H (2001) Responding phospholipid membranes–interplay between hydration and permeability. *Biophys J* 81(2):1014–1028.
35. ChemIDplus (2015) Dexamethasone in ChemIDplus database of United States National Library of Medicine (NLM). Available at chem.sis.nlm.nih.gov/chemidplus/rn/50-02-2. Accessed December 15, 2016.
36. Jepps OG, Dancik Y, Anissimov YG, Roberts MS (2013) Modeling the human skin barrier - towards a better understanding of dermal absorption. *Adv Drug Deliv Rev* 65(2):152–168.
37. Hashimoto K (1971) Intercellular space of the human epidermis as demonstrated with lanthanum. *J Invest Dermatol* 57(1):17–31.
38. Furuse M, et al. (2002) Claudin-based tight junctions are crucial for the mammalian epidermal barrier: A lesson from claudin-1-deficient mice. *J Cell Biol* 156(6):1099–1111.
39. Kubo A, Nagao K, Yokouchi M, Sasaki H, Amagai M (2009) External antigen uptake by Langerhans cells with reorganization of epidermal tight junction barriers. *J Exp Med* 206(13):2937–2946.
40. Kirschner N, Brandner JM (2012) Barriers and more: Functions of tight junction proteins in the skin. *Ann N Y Acad Sci* 1257(1):158–166.
41. Bicout DJ, Szabo A (1998) Electron transfer reaction dynamics in non-Debye solvents. *J Chem Phys* 109(6):2325–2338.
42. Nocedal J, Wright S (2006) *Numerical Optimization* (Springer, New York).
43. Conn AR, Gould NIM, Toint PL (2000) *Trust Region Methods* [Soc Industrial Appl Math (SIAM), Philadelphia].